

Macroscopic vs. microscopic models of circular Quantum Dots

J. Martorell

*Dept. d'Estructura i Constituents de la Materia, Facultat Física,
University of Barcelona, Barcelona 08028, Spain*

D. W. L. Sprung

*Department of Physics and Astronomy, McMaster University
Hamilton, Ontario L8S 4M1 Canada*

(Dated: May 14, 2021)

The confinement mechanism of electrons in gated circular quantum dots is studied in a sequence of models, from self-consistent 3D Hartree calculations to the semiclassical model of Shikin et al. Separation of the vertical from transverse confinement allows accurate 2D Hartree calculations. For moderate size dots containing ~ 50 electrons, 2D Thomas-Fermi can also be accurate. Finally, a Shikin type parameterization of the electron density allows quantitative study of the importance of the many contributions to the confinement potential.

PACS numbers: 73.21.La, 68.65.Hb

I. INTRODUCTION

Quantum dots defined by electrostatic confinement continue to be an important tool for exploring the physics of electrons on the mesoscopic scale. Numerous Coulomb blockade experiments have provided information on level spectra and capacitances. At present, more detailed knowledge is becoming available, since new experimental methods allow mapping of the charge distribution inside such dots and even the details of the individual electron wavefunctions can be resolved^{1,2,3,4,5}.

The most accurate electron wave functions are provided by 3D Poisson-Schrödinger simulations^{6,7,8}. These methods are highly developed but are computer intensive and therefore not well suited for systematic studies over a wide range of parameter values⁹. Furthermore, numerical results are seldom conducive to developing intuition about the importance of specific parameters. In parallel with these 3D approaches, a number of simpler two dimensional (2D) models have been developed^{10,11,12,13,14,15}. One of their key assumptions is strict confinement of the electron gas to a plane (2DEG), and often the transverse confining potential in that plane is taken arbitrarily to be a parabola or other simple analytic shape. Energy density functionals have been used to further simplify the computations while still including the main terms in the Hamiltonian. Free parameters available in such models can be adjusted to fit the data from the experiment being analyzed. The advantage of 2D models is that they require much less numerical effort, simplify the interpretation of results and allow systematic analysis. On the other hand, empirical parameters of these models may conceal or distort some aspects of the physics at play.

Our primary objective is to connect these two approaches in a detailed and quantitative manner. To do so with good accuracy and a reasonable amount of computation, we restrict our attention to axially symmetric dots, which has the advantage of reducing the number of

degrees of freedom.

The article is organized as follows: in Section II we describe the specific heterostructure layout that will be studied. We construct the total potential acting on the electrons, including the Coulomb interaction (direct and mirror terms), and the electrostatic confining potential due to the gates and donors. The resulting Hamiltonian is solved numerically in the 3D Hartree approximation. By varying the gate voltage we present results for dots of different sizes. Our first step towards simpler models with a more transparent interpretation is the factorization *ansatz* between longitudinal and transverse components of the electron wavefunctions. This describes the dot in an effective 2D Hartree approximation. We end this section by showing that the predictions of this *ansatz* are in very good agreement with the full 3D Hartree calculations.

Section III is devoted to the construction of effective confining potentials and coulomb interactions for use in 2D models, which incorporate finite thickness effects. We show in particular that there is a substantial difference at short distances between the effective Coulomb interaction and the $1/r$ law. In Section IV we define an energy density functional based on the Thomas-Fermi (T-F) approximation for the kinetic energy and, via a variational prescription, find equations to determine the corresponding electron density, along with the coulomb, confinement and kinetic energies.

In Section V, we show how to improve on the semiclassical model of Shikin *et al.*^{16,17}. We do so by taking into account the semiclassical kinetic energy, the mirror coulomb terms and the role of finite thickness of the 2DEG on the Coulomb interaction. We replace the Thomas-Fermi densities in the variational equations by the simple parametrization first introduced by Shikin *et al.*^{16,17} and later extended by Ye and Zaremba¹⁸. We show that after these simplifications, the numerical effort is reduced to a minimum: solving a very simple nonlinear equation for the dot radius R . The resulting predictions

for bulk properties such as the number of electrons, root mean square radius, kinetic, confining and Coulomb energies are quantitatively accurate. Finally, by restricting the parametrized density to the simplest Shikin form, but keeping all relevant potential contributions, we show that the dot size systematics can be obtained from an analytic expression where each term has a clear interpretation and expresses the physics quantitatively.

II. MICROSCOPIC MODELS: POISSON-SCHRÖDINGER.

A. The heterostructure

Fig. 1 shows a section of the heterojunction that we will use for reference. It consists of planar layers grown on a GaAs substrate which we model as infinitely thick and free of acceptors. From bottom to top there are 1) an AlGaAs spacer layer of thickness s , 2) an AlGaAs donor layer of thickness d , uniformly doped with donor concentration ρ_d , 3) a GaAs cap layer, undoped and of thickness c . The cap layer is covered by a metallic gate except for a circular opening of radius S_0 exposing the GaAs cap layer. Since our main purpose is to compare the predictions of several models, rather than to produce an accurate description of a specific experiment, we introduce several simplifying assumptions that will make our calculations less cumbersome, but which should not affect the physics to be explored. The first of these is the gate geometry just described. Using expressions to be given below, we have checked that for rings of a few hundred nanometers width, and same inner radius S_0 , the potential due to the gates is practically identical to that of the simplified gate used here, at the location of the dot. Also for simplicity we neglect the differences in dielectric constant ϵ_r between the different materials, and use a common energy-independent effective mass for spacer and substrate.

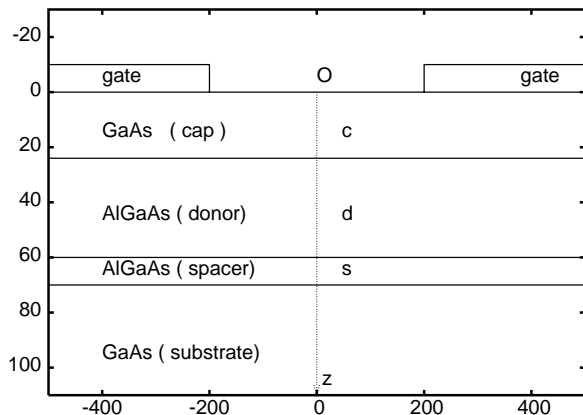


FIG. 1: Section of heterostructure layout. Lengths in nm.

Since in an earlier work¹⁹ we modelled quantum wires

using similar microscopic models we have adopted the same geometrical and physical parameters for the heterostructure: $c = 24$ nm, $d = 36$ nm, $s = 10$ nm, and $\rho_d = 6.10^{-4}$ nm⁻³, $\epsilon_r = 13.1$, $m^*/m_e = 0.067$. These values are taken from a model heterostructure considered by Laux *et al.*²⁰ in their pioneering work on wires. We have discussed how to deal with partially ionized donor layers in previous work¹⁹. Here for simplicity we will assume the donors are totally ionized. (This is often achieved in experiments by illuminating the sample.) Finally, we assume that the Fermi level is pinned at the exposed surface. This again would depend on how the sample has been processed, but for modelling purposes it has the advantage of being a definite prescription, which has been used frequently in a variety of problems^{7,21,22,23,24}. It is also a useful reference for other models of surface states^{25,26,27,28}. As indicated in Fig. 1, we choose the origin of coordinates at the center of the exposed surface, and the z axis orthogonal to the layers. Vectors from that axis, in planes parallel to the layers, are denoted by letters \vec{r} or \vec{s} . Following¹⁹, we construct the electrostatic potential acting on the electrons by adding the contributions from a) the gate, b) the ionized donor layer, and c) electrons in the dot. The potential due to a metallic gate, at voltage V_0 and with a circular hole of radius S_0 , can be derived from expressions given in Sect. 3.6 of²¹:

$$eV_g(\vec{r}, z) = \frac{1}{2\pi} \int d\vec{s} eV_g(\vec{s}, 0) \frac{|z|}{(z^2 + |\vec{r} - \vec{s}|^2)^{3/2}}, \quad (1)$$

where e is the electron charge ($e < 0$.) Using the boundary condition for Fermi level pinning,

$$eV_g(\vec{s}, 0) = eV_0 \Theta(s - S_0), \quad (2)$$

one finds, for $z > 0$,

$$eV_g(r, z) = eV_0 \frac{2z}{\pi} \int_{S_0}^{\infty} s ds E \left(\frac{4rs}{z^2 + (r+s)^2} \right) \frac{1}{z^2 + (r-s)^2} \frac{1}{(z^2 + (r+s)^2)^{1/2}}. \quad (3)$$

Here $E(k^2)$ is the complete elliptic integral of the second kind as defined in²⁹. To this one must add the electrostatic potential due to the donor layer, including the corresponding mirror term which maintains the boundary condition at the surface. As in¹⁹, in the substrate and spacer layers this contribution reduces to a constant additive term:

$$eV_d(z) = -\frac{e^2}{\epsilon} \rho_d d \left(c + \frac{d}{2} \right). \quad (4)$$

The third contribution is due to the Coulomb interaction between the electrons. Including the mirror terms it is:

$$eV_e(\vec{r}, z; \vec{r}', z') = \frac{e^2}{\epsilon_r} \left[\frac{1}{\sqrt{|\vec{r} - \vec{r}'|^2 + (z - z')^2}} - \frac{1}{\sqrt{|\vec{r} - \vec{r}'|^2 + (z + z')^2}} \right] \quad (5)$$

Appropriate band offsets in the AlGaAs layers, $eV_{bo} = 0.23$ eV, are included, but for brevity we do not write them in the expressions below. Choosing the Fermi level as the origin of energies and denoting by eV_s the binding energy of the surface states with respect to the conduction band edge, the latter will be located at:

$$eV_{g+d}(r, z) = eV_s + eV_g(r, z) + eV_d(z). \quad (6)$$

We have taken $eV_s = 0.7$ eV.

The Hamiltonian for N electrons in the dot is:

$$H = \sum_{i=1}^N \left(\frac{\hat{p}_i^2}{2m^*} + eV_{g+d}(r_i, z_i) \right) + \sum_{i<j=1}^N eV_e(\vec{r}_i, z_i; \vec{r}_j, z_j), \quad (7)$$

which we solve in the Hartree approximation.

B. 3D Hartree approximation

We take a trial product wave function

$$\Psi(\vec{r}_1, z_1; \dots; \vec{r}_N, z_N) = \prod_{i=1}^N \psi_i(\vec{r}_i, z_i), \quad (8)$$

and minimize the trial energy

$$E_H = \langle \Psi | H | \Psi \rangle, \quad (9)$$

under constraints that impose orthonormality of the orbitals ψ_i . To guarantee equilibrium with the surface states, all single particle states of negative energy are occupied. The variational method gives

$$\left[\frac{\hat{p}_i^2}{2m^*} + eV_{g+d}(r_i, z_i) + U_H(\vec{r}_i, z_i) \right] \psi_i = \varepsilon_i \psi_i(\vec{r}_i, z_i) \\ U_H(\vec{r}, z) = \int d\vec{r}' dz' eV_e(\vec{r}, z; \vec{r}', z') \rho(\vec{r}', z') \quad (10)$$

with

$$\rho(\vec{r}, z) = \sum_{i=1}^N |\psi_i(\vec{r}, z)|^2. \quad (11)$$

We will consider only dots with an even number of electrons. In that case the ground state solution has axial symmetry, so that

$$\rho(\vec{r}, z) = \rho(r, z) \quad , \quad U_H(\vec{r}, z) = U_H(r, z), \quad (12)$$

and the wavefunctions factorize as

$$\psi_{nl}(\vec{r}, z) = \frac{u_{nl}(r, z)}{\sqrt{r}} \frac{e^{i\ell\theta}}{\sqrt{2\pi}}. \quad (13)$$

We have omitted for simplicity the spin component of the wavefunction. Furthermore, eq. 10 simplifies to a two-dimensional Schrödinger equation

$$\varepsilon_{nl} u_{nl}(r, z) = -\frac{\hbar^2}{2m^*} \left(\frac{\partial^2}{\partial r^2} + \frac{\partial^2}{\partial z^2} \right) u_{nl}(r, z) + \left(eV_{g+d}(r, z) + U_H(r, z) + \frac{\hbar^2}{2m^*} \frac{l^2 - \frac{1}{4}}{r^2} \right) u_{nl}. \quad (14)$$

As usual, we have solved the system formed by eqs. 10 and 14 by numerical iteration. Before presenting results, we explore factorized approximate solutions of eq. 14.

C. Factorization ansatz

It is well known that large confining energies in the longitudinal direction support the validity of approximations where the z dependence in the wavefunctions is factored out from the other degrees of freedom. Guided by the success of the *ansatz* employed for linear wires¹⁹, we use it here for dots. We begin by approximating the two potential terms in eq. 14 as

$$eV_{g+d}(r, z) + U_H(\vec{r}, z) \simeq eV_{g+d}(0, z) + \overline{\Delta U}_c(r) + \overline{U}_H(\vec{r}) \quad (15)$$

where the effective two-dimensional confining, $\overline{\Delta U}_c$, and Hartree, \overline{U}_H , potentials are defined as:

$$\overline{\Delta U}_c(r) = \int dz A^2(z) (eV_{g+d}(r, z) - eV_{g+d}(0, z)) \\ \overline{U}_H(\vec{r}) = \int dz A^2(z) U_H(\vec{r}, z) \quad (16)$$

with a weight function $A^2(z)$ to be specified below. Formally the range of integration over z extends from $-\infty$ to $+\infty$, but in practice the $A(z)$ are non-zero only in the spacer and the substrate. Making these approximations in eq. 10 gives

$$\left[\frac{\hat{p}_z^2}{2m^*} + eV_{g+d}(0, z) + \overline{\Delta U}_c(r) + \overline{U}_H(\vec{r}) \right] \psi_i^{(a)} = \varepsilon_i^{(a)} \psi_i^{(a)} \quad (17)$$

that has solutions

$$\psi_i^{(a)}(\vec{r}, z) = A(z) \phi_i(\vec{r}), \quad (18)$$

with separately normalized $A(z)$ and ϕ_i , which satisfy Schrödinger equations with eigenvalues E_z and e_i

$$\left[\frac{\hat{p}_z^2}{2m^*} + eV_{g+d}(0, z) \right] A(z) = E_z A(z) \quad (19)$$

$$\left[\frac{\hat{p}_\perp^2}{2m^*} + \overline{\Delta U}_c(r) + \overline{U}_H(\vec{r}) \right] \phi_i(\vec{r}) = e_i \phi_i(\vec{r}) \quad (20)$$

Note that we have chosen the previously unspecified weight function $A(z)$ to be the common longitudinal component of the wavefunctions in 18. We then have

$$\varepsilon_i^{(a)} = E_z + e_i$$

$$E_H^{(a)} = NE_z + \sum_{i=1}^N \langle \phi_i | \frac{\hat{p}_1^2}{2m^*} + \overline{\Delta U}_c + \frac{1}{2} \overline{U}_H | \phi_i \rangle \quad (21)$$

The numerical process starts by constructing $eV_{g+d}(0, z)$ and solving eq. 19. After that $A(z)$ is fixed and we solve the two-dimensional Hartree problem iteratively, constructing the potentials from eqs. 16, and solving equation 20 for the $\phi_i(\vec{r})$, $i = 1, \dots, N$. For dots with an even number of electrons, axial symmetry allows separation of radial and angular factors in the $\phi_i(\vec{r})$, as done in eq. 13, and eq. 20 reduces to a one-dimensional equation for the radial components, which is straightforward to solve.

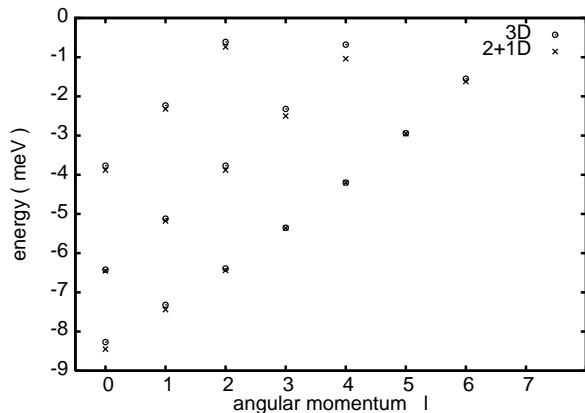


FIG. 2: Energies of single electron levels, corresponding to $V_0 = -1.27$ eV and $S_0 = 210$ nm. Circles: 3D Hartree, x symbols: factorization ansatz.

D. Results

In Fig. 2 we show, for $N = 54$ electrons, the orbital energies as a function of angular momentum. One sees that results using the factorization ansatz (labelled 2+1 D) are in excellent agreement with the exact Hartree (labelled 3 D). The various bulk energies are also accurately predicted by the factorization ansatz: To give two examples: 1) when $V_0 = -1.32$ V, we find a ground state with $N = 40$ electrons. The kinetic, confining, Coulomb and total energies are found to be 0.720 (0.729) eV, -3.263 (-3.272) eV, 1.215 (1.214) eV and -1.327 (-1.329) eV respectively. The quantities in parentheses correspond to the ansatz. 2) when $V_0 = -1.27$ V, $N = 54$, the respective values are 0.972 (0.985), -5.076 (-5.095), 1.947 (1.949) and -2.160 (-2.161) eV.

A 3D plot of the electron density $\rho(r, z)$ of the Hartree approximation shows that the dot extends about 20 nm along the z axis with a smooth variation very similar to the square of the Airy function. This will be exploited in Appendix A. Along r the density shows oscillations due

to filling of the various orbitals. This is displayed in Fig. 3 where we have plotted:

$$\sigma_H(r) \equiv \int \rho(r, z) dz. \quad (22)$$

for $N = 40, 54, 72$, and the corresponding quantity in the factorized approximation,

$$\sigma_H^{(a)}(r) = \sum_{i=1}^N |\phi_i(r)|^2. \quad (23)$$

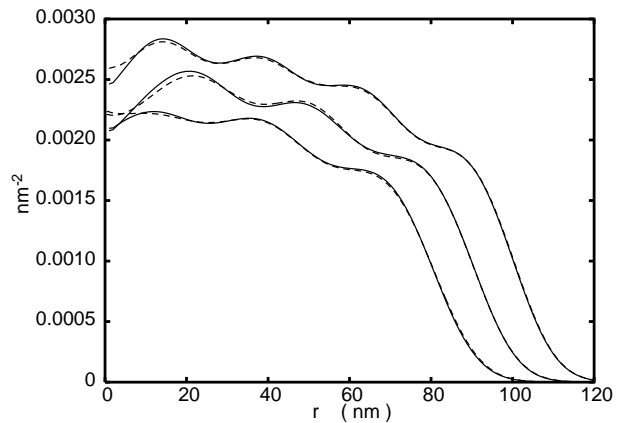


FIG. 3: 2D electron densities $\sigma(r)$ computed in the Hartree approximation (continuous lines) and the factorization ansatz (dashed lines). $N = 40, 54$ and 72 electrons.

Again, the agreement between the Hartree (3D) and the factorized densities is very good. A plot of the same densities of Fig. 3 on a logarithmic scale, shows that the agreement for the large r is excellent down to values as low as $\sigma_H(r) \simeq 10^{-6}$ nm $^{-2}$. This suggests that the factorization ansatz might be accurate in studies of tunneling across a ring of finite width. The root mean square radii are also accurately predicted: for $N = 40$ electrons we find 57.5 (57.6) nm, whereas for $N = 54$ the two values agree to three digits, 63.5 nm.

Fig. 4 shows the Hartree and confining potentials. Both are nearly parabolic for the radii corresponding to the area occupied by the dot ($r \leq 100$ nm), and their sum is almost constant in this range of r . We also find that the kinetic energy is small on the scale of the figure. These findings will be used in Sections IV and V to support, and improve on, the macroscopic model of Shikin *et al.*¹⁷.

III. POTENTIALS IN THE 2D LIMIT

Here, our aim is to develop the relation between the 3D calculations of the last section, and purely 2D models.

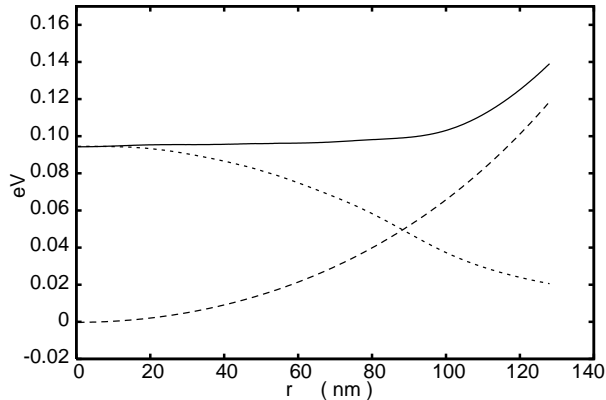


FIG. 4: 2D potentials $\Delta\bar{U}_c(r)$ (dashed line), $\bar{U}_H(r)$ (dotted line) and their sum (continuous line). $N = 54$, corresponding to $V_0 = -1.27$ eV and $S_0 = 210$ nm.

We make use of a separable expansion of the confining potential developed in Appendix B:

$$eV_g(r, z) = eV_g(0, z) + \frac{1}{2}k_c(z)r^2 + \frac{1}{2}k_4(z)r^4 \dots \quad (24)$$

Expressions for the coefficients are given in eq. B5. To have a workable expression for $\Delta\bar{U}_c(r)$ defined in eq. 16, we approximate the integral over z by replacing the exact $A(z)$ by Airy functions (see Appendix A). This leads to

$$\Delta\bar{U}_c(r) \simeq U_{2D,c}(r) \equiv \frac{1}{2}\bar{k}_c r^2 + \frac{1}{2}\bar{k}_4 r^4 \quad (25)$$

with the functions $k_c(z)$ and $k_4(z)$ replaced by their values at $z = \bar{z}$ given in eq. A12. From now on we will use this truncated form of the confining potential, $U_{2D,c}(r)$ with terms parabolic and quartic in r .

Guided by eq. 16, we define the effective 2D coulomb interaction as

$$\frac{\epsilon_r}{e^2} V_{2D}(|\vec{r} - \vec{r}'|) = \iint \frac{A^2(z)A^2(z') dz dz'}{\sqrt{|\vec{r} - \vec{r}'|^2 + (z - z')^2}}, \quad (26)$$

We now look for a suitable approximation that simplifies the averaging over the $A(z)$. To do so we again use that the $A(z)$ are well approximated by the Airy function. With notation introduced in Appendix A, we write

$$\frac{\epsilon_r}{e^2} V_{2D}(s) = \frac{\alpha}{(Ai'(\xi_0))^4} \iint \frac{Ai^2(u)Ai^2(u') du du'}{\sqrt{s^2\alpha^2 + (u - u')^2}}, \quad (27)$$

with $s = |\vec{r} - \vec{r}'|$. In this approximation, the ratio $V_{2D}(s)/\alpha$ depends only on the product $s\alpha$. The parameter α contains all the information on the confining potential and on the specific heterostructure. We have checked that to a very good approximation the effective interactions obtained numerically from eq. 26 for different values of S_0 and the gate potential V_0 also satisfy

this simple relation. The continuous line in Fig. 5 corresponds to the curves $(\epsilon_r/e^2) (V_{2D}(s)/\alpha)$ computed from eq. 26 for a range of values of S_0 from 150 to 260 nm and of V_0 from -1.12 to -1.42 V. On the scale of the figure they are all superimposed. The upper dashed line is for the pure $1/s$ potential and shows that the finite thickness effect (from averaging over $A(z)$) is substantial. For the simplified 2D models that we will introduce below, it will be very useful to have a simple analytic approximation for the effective interaction: empirically, we have found that the expression

$$\frac{\epsilon_r}{e^2} V_{2D}(s) = \frac{1}{\sqrt{s^2 + t^2(\alpha)}}. \quad (28)$$

with $t^2(\alpha) = 1/(2\alpha^2)$ gives a fairly good fit to the long range part of the interaction, and is very simple to use.

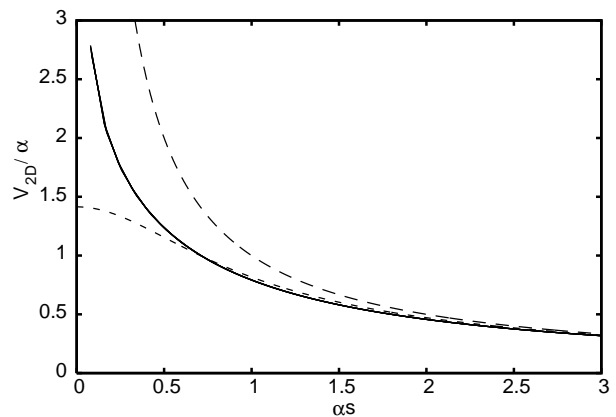


FIG. 5: Effective 2D Coulomb interactions. Continuous line: effective interactions defined in eq. 26. Upper long dashed line: $1/s$ interaction. Lower short dashed line: parametrization of eq. 28

Its physics content is also clear: we have replaced the $(z - z')^2$ in the denominator of eq. 26 by a constant, t , which plays the role of an effective thickness of the 2DEG. In this approximation the effective thickness is proportional to $\gamma^{-2/3}$, γ being the slope (in z) of the confining potential. In the following we will show that this effective interaction reproduces the direct Coulomb potential in the plane of the 2DEG very well.

A similar average has to be performed to define an effective mirror interaction. However, the width of the $A(z)$ functions is small compared to the value of $z + z' \simeq 2z_m \equiv D$, with $z = z_m$ the maximum of $A(z)$, and therefore it is a good approximation to write

$$\begin{aligned} \frac{\epsilon_r}{e^2} V_{2D,m}(|\vec{r} - \vec{r}'|) &= - \iint \frac{A^2(z)A^2(z') dz dz'}{\sqrt{|\vec{r} - \vec{r}'|^2 + (z + z')^2}} \\ &\simeq - \frac{1}{\sqrt{|\vec{r} - \vec{r}'|^2 + D^2}} \end{aligned} \quad (29)$$

IV. THE 2D ENERGY DENSITY FUNCTIONAL.

The Hartree approximation is expected to be valid when the number of electrons in the dot is not small. In that case, the kinetic energies involved are small compared to confinement and coulomb³⁰, and a Thomas-Fermi energy density functional becomes a sufficient approximation when the main interest is in the bulk properties of the system, rather than in details of each individual electron wavefunction and energy. Besides requiring much less numerical effort than solving eq. 20 for all the ϕ_i , this simpler model will allow us to obtain several analytic approximations that clarify the roles of the physical parameters of the system.

We replace the two-dimensional density constructed from the solutions of eq. 20 by its Thomas-Fermi approximation, $\sigma_{TF}(r)$. By definition the latter is to be determined from a variational condition on a suitably simplified expression for the total energy. Starting from eq. 21 we write

$$E_T = NE_z + E_{kin} + E_{con} + E_{Coul} \quad (30)$$

with

$$\begin{aligned} N &= \int \sigma_{TF}(r) d\vec{r} \\ E_{kin} &= \frac{\hbar^2}{2m^*} \pi \int \sigma_{TF}^2(r) d\vec{r} \\ E_{con} &= \int \overline{\Delta U}_c(r) \sigma_{TF}(r) d\vec{r} \\ E_{Coul} &= \frac{e^2}{2\epsilon_r} \int \left(V_{2D}(|\vec{r} - \vec{r}'|) + V_{2D,m}(|\vec{r} - \vec{r}'|) \right) \sigma_{TF}(r) \\ &\quad \cdot \sigma_{TF}(r') d\vec{r} d\vec{r}' , \end{aligned} \quad (31)$$

where we have used the well known expression for the kinetic energy E_{kin} of a 2D Thomas-Fermi gas. Defining now:

$$E(\mu) = E_T - \mu N \quad (32)$$

with a Lagrange multiplier μ to fix the number of electrons, the variational condition $\delta E(\mu)/\delta \sigma_{TF}$ leads to

$$\mu = E_z + \frac{\hbar^2}{m^*} \pi \sigma_{TF}(r) + \overline{\Delta U}_c(r) + \overline{U}_{H,TF}(r) \quad (33)$$

where:

$$\begin{aligned} \overline{U}_{H,TF}(r) &\equiv U_{2D,d}(r) + U_{2D,m} \\ &= \frac{e^2}{\epsilon_r} \int \left(V_{2D}(|\vec{r} - \vec{r}'|) + V_{2D,m}(|\vec{r} - \vec{r}'|) \right) \\ &\quad \cdot \sigma_{TF}(r') d\vec{r}' , \end{aligned} \quad (34)$$

These two equations define the iterative Thomas-Fermi approach. The process is started by solving the Schrödinger eq. 19 for $A(z)$ to determine E_z . Then $\overline{\Delta U}_c$

of eq. 25 is computed. The choice previously made for the origin of energies fixes $\mu = 0$. Then by iteratively solving eqs. 33 and 34 we determine σ_{TF} (and N). Note that we do take the longitudinal energy E_z into account in a realistic way, and therefore the 2D Fermi level of the dot is not 0 but $-E_z$. If we had taken it to be zero the results would be completely different.

We will not present the numerical results found in this approach, because they are very similar to those we will derive next, using parametrized analytic forms of the density. These prove to be more convenient for obtaining bulk properties in analytic form.

V. PARAMETRIZED DENSITIES

A. Extended Shikin model

The 2D Thomas-Fermi model is based on a semiclassical approximation for the kinetic energy. Some time ago, Shikin *et al.*^{16,17} noticed that the dominant contributions should be those of the coulomb and confining potentials and proposed a more drastic approximation: a model where both the kinetic energy contribution and mirror term were neglected in writing the total energy of the dot. Further they assumed that a parabolic confining potential

$$\overline{\Delta U}_c^S(r) = \frac{1}{2} k r^2 . \quad (35)$$

With these simplifications they obtained an analytic solution for the charge distribution:

$$\sigma_p(r) = \sigma_2 \sqrt{1 - \frac{r^2}{R^2}} \Theta(R - r) \quad (36)$$

with σ_2 and R given in terms of the parameters defining the potentials. Subsequently, Ye and Zaremba¹⁸ extended this model by adding quartic terms in the confining potential, and found the corresponding analytic solution for the electron distribution

$$\sigma_q(r) = \left[\sigma_2 \left(1 - \frac{r^2}{R^2} \right)^{1/2} + \sigma_4 \left(1 - \frac{r^2}{R^2} \right)^{3/2} \right] \Theta(R - r) . \quad (37)$$

We extend the above models by including accurate approximations for the contributions of the mirror potential, the thickness correction to the coulomb direct potential and the kinetic energy. We will show that one can still obtain analytic expressions and that our extension leads to results for bulk properties of the dots that compare very well with the Hartree calculations of the previous sections.

Let us begin by remembering that in the limit of a strictly two-dimensional quantum dot and a $1/r$ interaction, the direct coulomb potential corresponding to the

parametrized densities above is analytic

$$U_{2D,d}(r) = \frac{\pi^2 e^2}{2\varepsilon_r} R \left[\sigma_2 \left(1 - \frac{r^2}{2R^2} \right) \left(1 - \tau_2 \left(1 - \frac{r^2}{R^2} \right) \right) + \frac{3}{4} \sigma_4 \left(1 - \frac{r^2}{R^2} + \frac{3}{8} \frac{r^4}{R^4} \right) \left(1 - \tau_4 \left(1 - \frac{r^2}{R^2} \right) \right) \right], \quad \text{when } r \leq R, \quad (38)$$

and with the constants τ_2 and τ_4 equal to zero. In Appendix C we derive approximations for the direct potential which take into account the finite thickness of the dot using eq. 28. These approximations lead to the same expression, eq. 38, but with non-zero values for the constants τ_2 and τ_4 , which are given in eqs. C4 and C8.

The mirror potential can also be expressed in a simplified form, which is still sufficiently accurate, using eq. 29

$$\begin{aligned} U_{2D,m}(r) &= -\frac{e^2}{\varepsilon_r} \int d^2 r' \frac{\sigma_q(r')}{\sqrt{D^2 + |\vec{r} - \vec{r}'|^2}} \\ &\simeq -\frac{e^2}{\varepsilon_r} \int d^2 r' \frac{\sigma_q(r')}{\sqrt{D^2 + \frac{R_u^2}{2} + r^2}} \\ &= -\frac{e^2}{\varepsilon_r} \frac{N}{\sqrt{L^2 + r^2}}, \end{aligned} \quad (39)$$

where $L^2 = D^2 + R_u^2/2$. Note that we have replaced the $|\vec{r} - \vec{r}'|^2$ by its average over r' on a uniformly charged disk of radius R_u that contains the dot charge. The corresponding power series expansion is

$$U_{2D,m}(r) = -\frac{e^2 N}{\varepsilon_r L} \left(1 - \frac{r^2}{2L^2} + \frac{3}{8} \frac{r^4}{L^4} + \dots \right), \quad (40)$$

where according to eq. 37 the number of electrons is

$$N = \frac{2}{3} \pi R^2 \left[\sigma_2 + \frac{3}{5} \sigma_4 \right]. \quad (41)$$

Finally, for the small contribution of the kinetic energy term, we use the truncated expansion

$$\begin{aligned} \frac{\hbar^2 \pi}{m^*} \sigma_q &= \frac{\hbar^2 \pi}{m^*} \left[\sigma_2 \left(1 - \frac{r^2}{2R^2} - \frac{r^4}{8R^4} \right) + \sigma_4 \left(1 - \frac{3r^2}{2R^2} + \frac{3r^4}{8R^4} \right) \right]. \end{aligned} \quad (42)$$

With the approximations described above, eq. 33 can now be written as

$$E_z + U_{2D,c} + U_{2D,d} + U_{2D,m} + \frac{\hbar^2 \pi}{m^*} \sigma_q(r) = 0 \quad (43)$$

and should be satisfied for all $r \leq R$. Explicit forms for each of these terms have been written in eqs. 25, 38, 40 and 42. Equating the coefficients at each order of the power series, we arrive at

$$-E_z = \sigma_2 \left[\frac{\hbar^2 \pi}{m^*} + \frac{\pi^2 e^2}{2\varepsilon_r} R(1 - \tau_2) - \frac{2e^2 \pi}{3\varepsilon_r L} R^2 \right]$$

$$\begin{aligned} &+ \sigma_4 \left[\frac{\hbar^2 \pi}{m^*} + \frac{3\pi^2 e^2}{8\varepsilon_r} R(1 - \tau_4) - \frac{2e^2 \pi}{5\varepsilon_r L} R^2 \right] \\ -\frac{1}{2} \bar{k}_c &= \sigma_2 \left[-\frac{\hbar^2 \pi}{2m^* R^2} + \frac{\pi^2 e^2}{4\varepsilon_r R} (3\tau_2 - 1) + \frac{e^2 \pi}{3\varepsilon_r L^3} R^2 \right] \\ &+ \sigma_4 \left[-\frac{3\hbar^2 \pi}{2m^* R^2} + \frac{3\pi^2 e^2}{8\varepsilon_r R} (2\tau_4 - 1) + \frac{e^2 \pi}{5\varepsilon_r L^3} R^2 \right] \\ -\frac{1}{2} \bar{k}_4 &= \sigma_2 \left[-\frac{\hbar^2 \pi}{8m^* R^4} - \frac{\pi^2 e^2}{4\varepsilon_r R^3} \tau_2 - \frac{e^2 \pi}{4\varepsilon_r L^5} R^2 \right] \\ &+ \sigma_4 \left[\frac{3\hbar^2 \pi}{8m^* R^4} + \frac{3\pi^2 e^2}{64\varepsilon_r R^3} (3 - 11\tau_4) - \frac{3e^2 \pi}{20\varepsilon_r L^5} R^2 \right], \end{aligned} \quad (44)$$

which is a system of equations in three unknowns: σ_2 , σ_4 and R . Since the equations are linear, one can eliminate σ_2 and σ_4 leaving a single nonlinear equation in R , which is then solved numerically, by Newton-Raphson. We have already seen that for each value of V_0 one finds a corresponding E_z . Therefore, for each V_0 , eqs. 44 determine a set σ_2, σ_4 and R , and these give N and other quantities such as the mean square radius

$$\langle r^2 \rangle = \frac{4\pi R^4}{5N} \left(\frac{\sigma_2}{3} + \frac{\sigma_4}{7} \right), \quad (45)$$

or the various energies

$$\begin{aligned} E_{con} &= \int d^2 r U_{2D,c}(r) \sigma_q(r) = \pi R^4 \left[\sigma_2 \left(\frac{2}{15} \bar{k}_c + \frac{8}{105} \bar{k}_4 R^2 \right) + \sigma_4 \left(\frac{2}{35} \bar{k}_c + \frac{8}{315} \bar{k}_4 R^2 \right) \right], \quad (46) \\ E_{Coul,d} &= \frac{1}{2} \int d^2 r U_{2D,d}(r) \sigma_q(r) = \frac{\pi^3 e^2 R^3}{4\varepsilon_r} \\ &\cdot \left[\sigma_2^2 \frac{4}{5} \left(\frac{2}{3} - \frac{3}{7} \tau_2 \right) + \sigma_4^2 \frac{1}{35} \left(8 - \frac{19}{3} \tau_4 \right) + \sigma_2 \sigma_4 \frac{1}{7} \left(\frac{24}{5} - \frac{16}{9} \tau_2 - \frac{9}{5} \tau_4 \right) \right] \\ E_{Coul,m} &= \frac{1}{2} \int d^2 r U_{2D,m}(r) \sigma_q(r) = -\frac{e^2 \pi N}{\varepsilon_r L} R^2 \left[\sigma_2 \left(\frac{1}{3} - \frac{R^2}{15L^2} + \frac{R^4}{35L^4} \right) + \sigma_4 \left(\frac{1}{5} - \frac{R^2}{35L^2} + \frac{R^4}{105L^4} \right) \right] \\ E_{kin} &= \int d^2 r \frac{\hbar^2 \pi}{2m^*} \sigma_q^2(r) \\ &= \frac{\hbar^2 \pi^2}{2m^*} R^2 \left[\frac{1}{2} \sigma_2^2 + \frac{2}{3} \sigma_2 \sigma_4 + \frac{1}{4} \sigma_4^2 \right] \end{aligned} \quad (47)$$

In Figs. 6 to 10 we compare the results of the present model to our Hartree calculations (with the separation ansatz). Fig. 6 shows the number of electrons versus the gate potential. The prediction (long dashed line) is so close to the Hartree results that the two lines can only be distinguished when eV_0 is close to 1.1 eV. For comparison we also show the predictions when the finite thickness corrections, or the quartic terms, are omitted. As

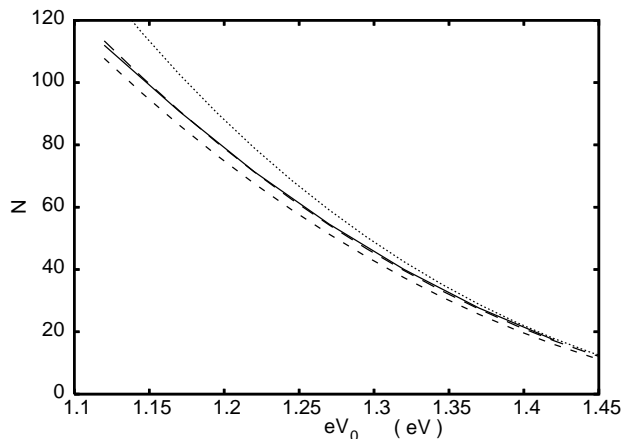


FIG. 6: Electron number N obtained from the various models: continuous line: factorized Hartree. Long dashed line overlapping with it on most of the range: parametrized density, $\sigma_q(r)$, with parameters determined as described in Section V. Short dashed line underneath: same but omitting the non-zero thickness corrections in the coulomb terms ($\tau_2 = \tau_4 = 0$.) Upper dotted line: same but omitting the quartic term in the confining potential ($k_4 = 0$).

expected, the quartic terms are relevant only for large dots, whereas the finite size correction is sizeable even for small ones. Fig. 7 shows the evolution of the various energies per particle: Coulomb (direct plus mirror), confining and kinetic, as eV_0 is varied. Again the agreement is excellent, confirming the validity of the model for bulk properties. The agreement is even better for the fields: for the example shown in Fig. 4, those given by the parametrized densities are so close that they cannot be distinguished from those plotted in the figure. This is a very useful result, since one can use them as starting values for self-consistent solution of the Hartree equations, and convergence is then very fast.

Fig. 8 shows the root mean square radii. Again the variation with V_0 is fairly well reproduced. But one observes a small systematic underestimate that we now examine for a specific case. Fig. 10 compares the radial distributions of charge for a gate voltage of $V_0 = -1.22$ V. As expected, the quantal oscillations of the Hartree density are more pronounced than those from the parametrized density. However, the most significant disagreement occurs at the surface, where the form of σ_q only allows an interpolation between the oscillations of σ_H . This is clearly shown by their difference, the dotted line in that figure. Still it is seen that most of the charge is correctly located, and this is why the energies and fields are so accurately predicted by the model.

Fig. 9 is a more detailed plot of relevant energies v.s. V_0 . We show separately the contributions from the direct and mirror Coulomb terms. The mirror term is quite large and should not be ignored in any 2D calculation. We also show three comparatively small terms: the ki-

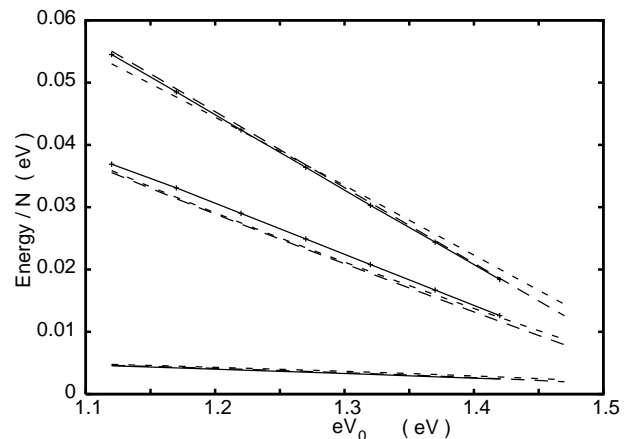


FIG. 7: Energies per electron v.s. gate voltage. From top to bottom: Coulomb, confining and kinetic. Continuous lines: Hartree with factorization ansatz. Long dashed lines: predictions of parametrized densities of eq. 37 and expressions 46 to 47. Short dashed lines: analytic approximations: eqs. 54.

netic energy (positive), the Coulomb exchange (negative) and the correction to Coulomb due to the finite thickness of the 2DEG. The latter correction is obtained from the expression for the Coulomb energy in eq. 47 as

$$\Delta E_{Coul,d} = E_{Coul,d} - E_{Coul,d}(\tau_2 = 0, \tau_4 = 0) . \quad (48)$$

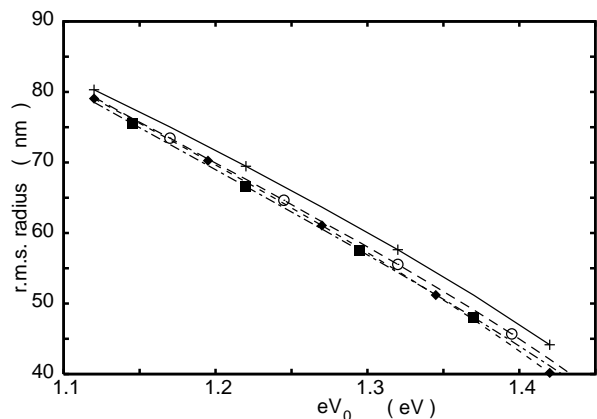


FIG. 8: Root mean square radius v.s. gate voltage. Continuous line with “+” signs: Hartree, (factorization ansatz). Dashed line with circles: parametrized density with two terms. Dotted line with diamonds: parametrized density with one term, eq. 51. Dash-dotted line with boxes: prediction of eq. 52.

For comparison, the Coulomb exchange energy has also been computed following Zaremba³¹, although the effect of the corresponding effective potential has not been

included in our model. Notice that its contribution is comparable to the effect of the finite thickness on the Coulomb energy, a term that pure 2D models neglect.

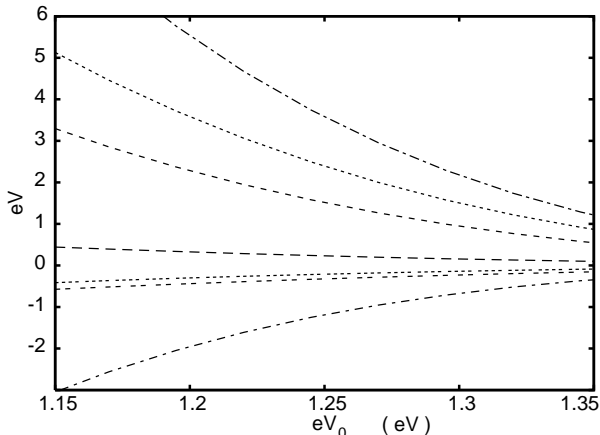


FIG. 9: Energies relevant to the equilibrium configurations v.s. V_0 : from top to bottom: Coulomb direct, Coulomb direct plus mirror, confining, kinetic, Coulomb finite thickness effect, Coulomb exchange and Coulomb mirror terms.

B. Analytic approximations for the radii and bulk energies

The values of σ_4 are typically about ten percent of those of σ_2 . Therefore, if one is willing to trade some accuracy for simplicity, σ_4 can be neglected. In this approximation, $\sigma_q(r)$, eq. 37, is replaced by $\sigma_p(r)$ of eq. 36 and the direct coulomb potential reduces to:

$$U_{2D,d} = \frac{\pi^2 e^2}{2\varepsilon_r} R \sigma_2 \left(1 - \tau_2 + \frac{1}{2}(3\tau_2 - 1) \frac{r^2}{R^2} - \frac{\tau_2}{2} \frac{r^4}{R^4} \right), \quad (49)$$

which, due to the smallness of τ_2 , is practically parabolic. It is clear then that imposing eq. 43 for all $r \leq R$ will lead to unphysical results. What we do instead is to impose it a) as a weighted average over all r , with $\sigma_p(r)$ as weight function and b) at $r = 0$, where the quartic terms are not relevant. We then arrive at two equations:

$$\begin{aligned} -E_z &= \frac{1}{5} \bar{k}_c R^2 + \frac{4}{35} \bar{k}_4 R^4 + \sigma_2 \left[\frac{3\hbar^2 \pi}{4m^*} \right. \\ &+ \left. \frac{3\pi^2 e^2}{5\varepsilon_r} R \left(\frac{2}{3} - \frac{3}{7} \tau_2 \right) - \frac{2\pi e^2}{\varepsilon_r} \frac{R^2}{L} \left(\frac{1}{3} - \frac{R^2}{15L^2} + \frac{R^4}{35L^4} \right) \right] \\ -E_z &= \sigma_2 \left(\frac{\hbar^2 \pi}{m^*} + \frac{\pi^2 e^2}{2\varepsilon_r} R(1 - \tau_2) - \frac{2\pi e^2}{3\varepsilon_r} \frac{R^2}{L} \right) \end{aligned} \quad (50)$$

which can again be reduced to a single non-linear equation for R :

$$R^2 = -E_z \frac{1 - \frac{17}{7} \tau_2 - \frac{4}{\pi} \frac{R^3}{L^3} \left(\frac{1}{3} - \frac{R^2}{7L^2} \right) + 5\xi_k}{\left(\bar{k}_c + \frac{4}{7} \bar{k}_4 R^2 \right) (1 - \tau_2 - \frac{4}{3\pi} \frac{R}{L} + 4\xi_k)} \quad (51)$$

where $\xi_k \equiv \hbar^2 / (2m^*) \varepsilon_r / (\pi e^2 R) \simeq 1.65/R$ is the small correction due to the kinetic energy. Similarly the finite thickness corrections are only a few percent. Note also that in both cases there is a significant cancellation between the corrections in the numerator and in the denominator, so to a first approximation they cancel. By neglecting the mirror and the quartic term contributions one arrives at Shikin's simple result

$$R_S^2 = -\frac{E_z}{\bar{k}_c}. \quad (52)$$

Due to other cancellations that we will discuss below, R_S is fairly close to the value of R found by solving eq. 51 without simplification. This is shown in Fig. 8. To give a specific example, when $V_0 = -1.27$ V, the value of R from eq. 44 is 98.0 nm, the value from eq. 51 is 96.5 nm, and from eq. 52 $R_S = 95.8$ nm. One can thus find a good approximate solution for R by inserting R_S for R on the rhs of eq. 51. This gives $R = 96.6$ nm, and on the scale of Fig. 8 the exact and the approximate solutions to eq. 51 are indistinguishable. The agreement with the Hartree results is also quite good. This clearly shows that eqs. 51 and 52 can be used to quantify the effect of the different terms on the size of the dot.

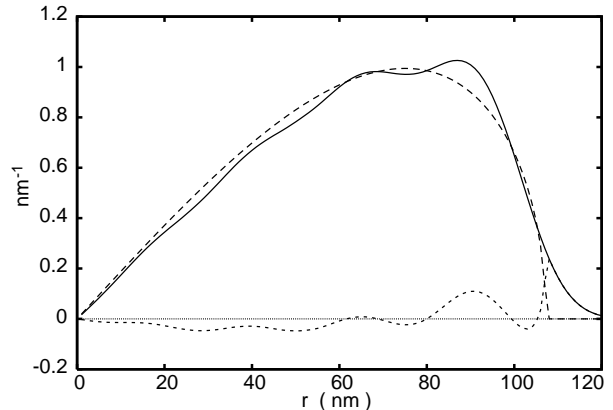


FIG. 10: Radial distribution of charges: Densities weighted with a factor $2\pi r$, for $V_0 = -1.22$ V. Continuous line: Hartree with factorization ansatz. Dashed line: parametrized density, eq. 37. Dotted line: difference.

Expanding the second denominator in eq. 51 and neglecting small terms gives

$$R^2 \approx R_S^2 \left(1 - \frac{10}{7} \tau_2 + \frac{4}{3\pi} \frac{R_S}{L_S} - \frac{4}{7} \frac{\bar{k}_4 R_S^2}{\bar{k}_c} + \xi_k \right), \quad (53)$$

which is less accurate, particularly for large dots. But, the usefulness of this simplified expression is that it displays very simply the expected role of each contribution: the finite thickness correction and the confining quartic term decrease the radius, whereas the mirror term increases it. For our chosen heterostructure, cancellations

between the contributions to eq. 53 leave the final dot size very close to R_S . The dependence of R_S on V_0 can be brought out using analytic expressions from the appendices: the numerator of eq. 52, E_z , can be approximated by eq. A2, whereas the denominator is linear in V_0 as shown in eq. B5. From these expressions, the predicted values of R_S fall between the continuous line in Fig. 8 describing the Hartree results and the dashed line corresponding to solutions of eq. 51. Summarizing: due to mutually compensating effects, the main trends in the dependence of the dot size on the gate voltage can be easily understood with the help of the expressions given in the appendices for the numerator and denominator of eq. 52. A similar analysis can be made for the corrections to σ_2 using the second of eqs. 50. Then from eqs. 46 and 47 we find

$$\begin{aligned} \frac{E_{Coul}}{N} &= -E_z \left[\frac{2}{5} \frac{1 - \frac{9}{14}\tau_2}{1 - \tau_2 - \frac{4}{3\pi} \frac{R}{L} + 2 \frac{\hbar^2}{m^*} \frac{\epsilon_r}{\pi e^2 R}} \right. \\ &\quad \left. - \frac{2}{3\pi} \frac{R}{L} \frac{1 - \frac{R^2}{5L^2} + \frac{R^4}{7L^4}}{1 - \tau_2 - \frac{4R}{3\pi L}} \right] \\ \frac{E_{con}}{N} &= \frac{R^2}{5} \left(\bar{k}_c + \frac{4}{7} \bar{k}_4 R^2 \right) \\ \frac{E_{kin}}{N} &= -E_z \frac{\frac{3}{8} \frac{\hbar^2 \pi}{m^*}}{\frac{\hbar^2 \pi}{m^*} + \frac{\pi^2 e^2}{2\epsilon_r} R(1 - \tau_2) - \frac{2\pi e^2 R^2}{3\epsilon_r L}}. \end{aligned} \quad (54)$$

Setting $R = R_S$ and using the analytic expression for E_z , eq. A2, the predictions are as shown in Fig. 7: they are quite accurate, so that one can see by inspection of eqs. 54 the role of each term in determining the bulk energies given by the 3D Hartree calculations.

VI. SUMMARY AND CONCLUSIONS

Starting from a 3D Poisson-Schrödinger model, we have studied a sequence of approximations. The 3D Hartree results show that although the electrons are confined around the junction plane, they are spread longitudinally more than 20 nm into the substrate. We have introduced a factorization *ansatz* that is very accurate, by factorizing out a common longitudinal component of the wavefunctions, as a first step towards pure 2D models. In the second half of the manuscript we have focussed on improving the semi-classical model of Shikin *et al.*¹⁷. We have formulated a variational approach where in addition to the classical ingredients, (confinement and direct Coulomb potentials), we take into account the kinetic energy via the Thomas Fermi approximation, the mirror coulomb terms and the finite thickness of the 2DEG. We have shown that using parametrized densities in the variational equations leads to good values for the number

of electrons, mean square radius, kinetic, confining and Coulomb energies. Furthermore, the corresponding total potential seen by the electrons is so close to that found in the Hartree factorization *ansatz*, that it provides a very efficient starting point for full Hartree calculations. In an additional simplifying step we have shown that choosing the simplest parametrization for the density, but keeping all potential contributions, the dependence of the bulk properties on the gate voltage can be described analytically. These expressions clarify the role of each parameter in determining the dot properties. This detailed and quantitative connection between 3D simulations and the simplest 2D models provides an essential tool for discussing the systematics of bulk quantum dot properties in a transparent and intuitive way.

Acknowledgments

We are grateful to NSERC-Canada for Discovery Grant RGPIN-3198 (DWLS), and to DGES-Spain for continued support through grants FIS2004-03156 and FIS2006-10268-C03-02 (JM).

APPENDIX A: APPROXIMATE LONGITUDINAL WAVEFUNCTIONS

1. Airy functions

Here we describe how we approximate the longitudinal wavefunctions $A(z)$, by Airy functions. It is well known that the potential term $eV_{g+d}(0, z)$ is close to linear in the substrate, and a steep barrier in the spacer layer. Therefore, in the substrate we approximate eq. 19 by

$$-\frac{\hbar^2}{2m^*} A_l''(z) + \gamma(z - z_J) A_l(z) = E_l A_l(z) \quad (A1)$$

where z_J is the location of the junction between substrate and spacer, and γ a constant slope whose value will be fixed below. In this approximation:

$$E_z = E_l + eV_s - \frac{4\pi e^2}{\epsilon_r} \rho_d d \left(c + \frac{d}{2} \right) + eV_0 \frac{z_J}{\sqrt{z_J^2 + S_0^2}}. \quad (A2)$$

Introducing the change of variables

$$u = \alpha(z - z_J) + \xi_0, \quad (A3)$$

with the identifications

$$\begin{aligned} \alpha &= \left(\frac{2m^* \gamma}{\hbar^2} \right)^{1/3} \\ E_l &= -\xi_0 \gamma^{2/3} \left(\frac{\hbar^2}{2m^*} \right)^{1/3}, \end{aligned} \quad (A4)$$

eq. A1 reduces to the Airy equation in the form given on page 446 of Abramowitz and Stegun²⁹

$$A_l''(u) - uA_l(u) = 0. \quad (\text{A5})$$

In the limit of an infinitely steep spacer barrier, $A_l(z)$ must vanish at $z = z_J$ so the first zero of the Airy function $Ai(u)$ must occur at this point. Since the location of that zero is at $\xi_0 = -2.33810$, the form of $A_l(z)$ is completely determined.

$$A_l(z) = \mathcal{N} Ai(\alpha(z - z_J) + \xi_0) \Theta(z - z_J). \quad (\text{A6})$$

The normalization, and the location of the maximum are also analytic

$$\begin{aligned} \mathcal{N} &= \frac{\sqrt{\alpha}}{Ai'(\xi_0)} \\ z_m &= z_J + \frac{1}{\alpha}(\xi'_0 - \xi_0), \end{aligned} \quad (\text{A7})$$

with $\xi'_0 = -1.01879$. To have a good approximation for the potential where the wavefunction is largest, we choose to define the slope γ as

$$\gamma \equiv \left[\frac{d(eV_{g+d}(0, z))}{dz} \right]_{z=z_m} = eV_0 \frac{S_0^2}{(z_m^2 + S_0^2)^{3/2}}. \quad (\text{A8})$$

For a given V_0 , and the $A(z)$ determined by solving eq. 19, we construct its analytic approximation by shifting $A_l(z)$ to make the maxima of the two coincide. In Fig. 11 we compare the shifted $A_l(z)$ to the numerically determined $A(z)$ for a representative gate voltage. One sees that the A_l forbid tunneling into the spacer, but that their shape in the substrate is correct.

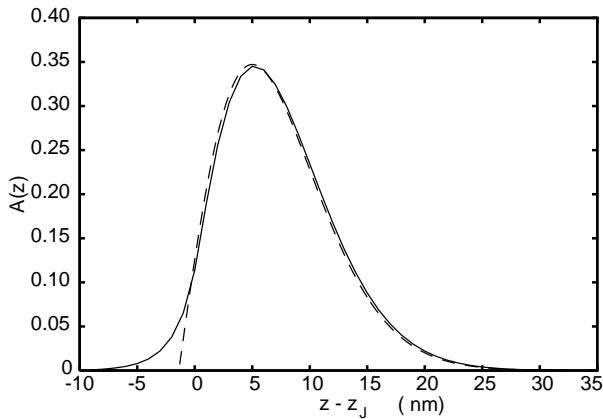


FIG. 11: Longitudinal wavefunction as determined using the factorization ansatz (continuous line), compared to the Airy approximation described in Appendix A (dashed line.) $V_0 = -1.27$ V.

2. Averages over z

As will be shown in Appendix B, eq. B5, the confining potential can be expanded as a power series in r^2 . To extract from it an effective 2D confining potential using eq. 16 one has to perform an average over z with weight function $A^2(z)$. We approximate this average using the $A_l(z)$. For the quadratic term one has to determine:

$$\bar{k}_c \equiv eV_0 \frac{3S_0^2}{2} \int \frac{z}{(z^2 + S_0^2)^{5/2}} A^2(z) dz, \quad (\text{A9})$$

and in this expression the denominator varies little ($z^2 \ll S_0^2$) in the range where $A(z)$ is nonvanishing. We remove it from the integral, leaving an average

$$\int z A^2(z) dz \simeq z_J + \int (z - z_J) A_l^2(z) dz = z_J - \frac{2}{3} \frac{\xi_0}{\alpha}. \quad (\text{A10})$$

Combining this approximation with the second of eqs. A7 we find:

$$\bar{k}_c = k_c(\bar{z}) = \frac{3}{2} eV_0 \frac{\bar{z} S_0^2}{(\bar{z}^2 + S_0^2)^{5/2}}, \quad (\text{A11})$$

with

$$\bar{z} = z_m - \frac{\xi'_0 - \xi_0}{\alpha} - \frac{2}{3} \frac{\xi_0}{\alpha}, \quad (\text{A12})$$

where z_m is the location of the maximum of $A(z)$. The quartic term in the confining potential can also be approximated with the same prescription, neglecting the variation with z in the denominator of the r^4 term in eq. B5 and keeping only the dependence on z in the numerator.

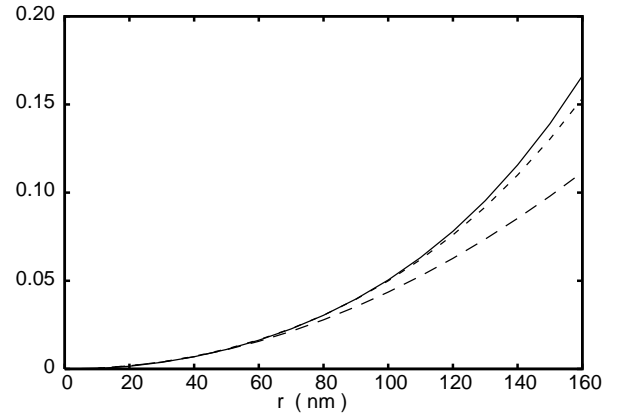


FIG. 12: Confining potential $(V_g(r, z) - V_g(0, z))/V_0$ (solid line) compared to the power series expansion in r^2 with one (long dashed line) and two terms (short dashed line). $z = 70$ nm in this example.

APPENDIX B: POWER SERIES EXPANSION OF THE GATE POTENTIAL

From eqs. 1 and 2, when $z > 0$ we have

$$eV_g(r, z) \equiv \frac{eV_0}{2\pi} \int_{S_0}^{\infty} s ds \int_0^{2\pi} d\theta \frac{z}{(z^2 + |\vec{r} - \vec{s}|^2)^{3/2}}, \quad (\text{B1})$$

To determine the series expansion in powers of r for fixed z , we use an auxiliary expansion that generates the derivatives $\partial^n(eV_g)/\partial r^n$ in a straightforward way. We expand

$$\begin{aligned} [z^2 + |\vec{r} - \vec{s}|^2]^{-3/2} &= [z^2 + s^2 - 2rs \cos \theta + r^2]^{-3/2} \\ &= (z^2 + s^2)^{-3/2} \left[1 - \frac{2rs \cos \theta - r^2}{z^2 + s^2} \right]^{-3/2} \\ &\simeq (z^2 + s^2)^{-3/2} \left(1 + \frac{3}{2} \frac{2rs \cos \theta - r^2}{z^2 + s^2} \right. \\ &\quad \left. + \frac{15}{8} \left(\frac{2rs \cos \theta - r^2}{z^2 + s^2} \right)^2 + \dots \right), \end{aligned} \quad (\text{B2})$$

and integrate over θ term by term. To illustrate the steps we write only the first three terms in the expansion. The integration over θ gives

$$\begin{aligned} eV_g(r, z) &= eV_0 z \int_{S_0}^{\infty} s ds \left[\frac{1}{(z^2 + s^2)^{3/2}} - \frac{3}{2} \frac{r^2}{(z^2 + s^2)^{5/2}} \right. \\ &\quad \left. + \frac{15}{4} \frac{r^2 s^2}{(z^2 + s^2)^{7/2}} + \frac{15}{8} \frac{r^4}{(z^2 + s^2)^{7/2}} \right]. \end{aligned} \quad (\text{B3})$$

These integrals are analytical, so that

$$\begin{aligned} eV_g(r, z) &= eV_0 \left[\frac{z}{\sqrt{z^2 + S_0^2}} + \frac{3}{4} \frac{z S_0^2}{(z^2 + S_0^2)^{5/2}} r^2 \right. \\ &\quad \left. + \frac{3}{8} \frac{z}{(z^2 + S_0^2)^{5/2}} r^4 \right] \end{aligned} \quad (\text{B4})$$

To get all the contributions of order r^4 , one has to include two more terms in the expansion of eq. B2. We skip the details and quote the full result

$$\begin{aligned} eV_g(r, z) &= eV_0 \left[\frac{z}{(z^2 + S_0^2)^{1/2}} + \frac{3}{4} \frac{z S_0^2}{(z^2 + S_0^2)^{5/2}} r^2 \right. \\ &\quad \left. + \frac{15}{64} \frac{z S_0^2 (-4z^2 + 3S_0^2)}{(z^2 + S_0^2)^{9/2}} r^4 + \dots \right], \end{aligned} \quad (\text{B5})$$

In Fig. 12 we show the various results for $(V_g(r, z) - V_g(0, z))/V_0$ for $z = z_J = 70$ nm, as a function of r . As can be seen, the power series converges nicely towards the exact result. We have checked that similar convergence holds for other values of z .

APPENDIX C: FINITE THICKNESS CORRECTIONS

Here we derive the effective Coulomb potential to be used when treating the dot as a 2DEG. We first compute the exact correction at $r = 0$ for the two terms of the parametrized density, eq. 37. Then we show that to a good approximation a simple parametrization based on this correction can be used when $r \neq 0$.

1. Potentials at $r = 0$

Using the effective interaction defined in eq. 28, and the first term of the parametrized density, the potential that we wish to compute requires the integral

$$I(t) = 2 \int_0^R \frac{\sqrt{1 - r^2/R^2}}{\sqrt{r^2 + t^2}} r dr. \quad (\text{C1})$$

With the change of variable: $x = r^2$, the integral takes a form that can be easily evaluated:

$$I(t) = -t + R \left(1 + \frac{t^2}{R^2} \right) \left(\frac{\pi}{2} - \arctan \frac{t}{R} \right). \quad (\text{C2})$$

and when $t^2/R^2 \ll 1$

$$I(t) \simeq -t + R \left(\frac{\pi}{2} - \frac{t}{R} \right) = \frac{\pi R}{2} - 2t, \quad (\text{C3})$$

so that defining

$$\tau_2 = \frac{4t}{\pi R} \quad (\text{C4})$$

one can finally write the finite thickness correction as $I(t) = (1 - \tau_2)I(t=0)$. We have checked numerically that indeed this approximation is quite good for the usual values of R and the value of t given in eq. 28.

For the second term of σ_q , eq. 37, the integral of interest is

$$\begin{aligned} I_q(t) &= 2 \int_0^R \frac{(1 - r^2/R^2)^{3/2}}{\sqrt{r^2 + t^2}} r dr = \\ &= \int_0^{R^2} \frac{(1 - x/R^2)^{3/2}}{\sqrt{x + t^2}} dx \\ &= \int_0^{R^2} \frac{(1 - x/R^2)^2 dx}{\sqrt{(x + t^2)(1 - x/R^2)}}, \end{aligned} \quad (\text{C5})$$

Making use of integrals found on page 83 of³², we arrive at

$$\begin{aligned} I_q(t) &= \frac{3}{8} R \left(\frac{\pi}{2} + \arcsin \frac{R^2 - t^2}{R^2 + t^2} \right) \left(1 + \frac{t^2}{R^2} \right)^2 \\ &\quad - t \left(\frac{5}{4} + \frac{3t^2}{4R^2} \right). \end{aligned} \quad (\text{C6})$$

This result reduces to $I_q(t=0) = 3\pi R/8$ in the limit $t=0$, for which the integration is trivial. Then we define $\zeta_4 \equiv I_q(t)/I_q(0)$, and write

$$\zeta_4 = \frac{8}{3\pi} \left[\frac{3}{8} \left(\frac{\pi}{2} + \arcsin \frac{R^2 - t^2}{R^2 + t^2} \right) \cdot \left(1 + \frac{t^2}{R^2} \right)^2 - \frac{t}{4R} \left(5 + 3 \frac{t^2}{R^2} \right) \right]. \quad (\text{C7})$$

If $t^2/R^2 \ll 1$ can be neglected, the expression for ζ_4 simplifies to

$$\zeta_4 \equiv 1 - \tau_4 = 1 - \frac{10}{3\pi} \frac{t}{R}. \quad (\text{C8})$$

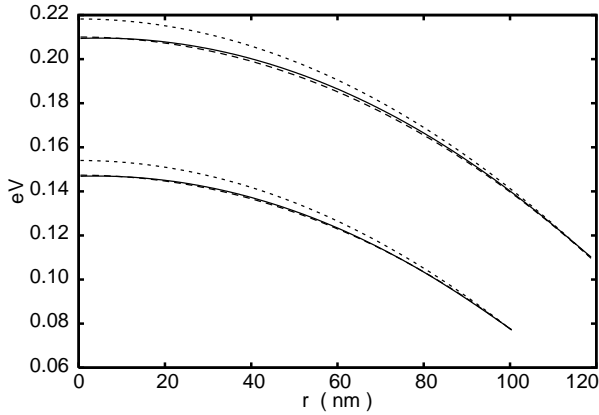


FIG. 13: Direct Coulomb potential for the first term of the parametrized densities $\sigma_q(r)$, eq. 37. Values of σ_2 corresponding to $V_0 = -1.17$ V (top) and $V_0 = -1.27$ V (bottom.) Continuous lines: exact numerical calculation using eqs. 26 and 34. Dotted lines: zero thickness eq. C9; dashed lines: including the finite thickness correction: eq. C10.

2. The direct Coulomb potential when $r \neq 0$

When the 2D interaction is taken as $1/r$ the Coulomb potential for the density $\sigma_p(r)$ is analytic:

$$U_{2D,d}(r) = \frac{\pi^2 e^2}{2\epsilon_r} R \sigma_2 \left(1 - \frac{r^2}{2R^2} \right). \quad (\text{C9})$$

In Fig. 13 we compare this curve, dotted lines, to the exact numerical calculation using eqs. 26 and 34. As expected there is a sizeable discrepancy where the dot charge is large, and as the distance from the center of the dot increases the thickness effect decreases. The dashed lines are our empirical prescription for extending the finite thickness correction to non vanishing r :

$$U_{2D,d}^{(2)}(r) = \frac{\pi^2 e^2}{2\epsilon_r} R \sigma_2 \left(1 - \frac{r^2}{2R^2} \right) \left(1 - \tau_2 \left(1 - \frac{r^2}{R^2} \right) \right) \quad (\text{C10})$$

As shown in Fig. 13, this prescription accurately reproduces the exact calculations. For the small contribution of the second term in the parametrized density we use a similar prescription:

$$U_{2D,d}^{(4)}(r) = \frac{3\pi^2 e^2}{8\epsilon_r} R \sigma_4 \left(1 - \frac{r^2}{R^2} + \frac{3}{8} \frac{r^4}{R^4} \right) \times \left(1 - \tau_4 \left(1 - \frac{r^2}{R^2} \right) \right), \quad (\text{C11})$$

and the results (not shown) are also sufficiently accurate.

¹ R. Crook, C.G. Smith, M.Y. Simmons and D.A. Ritchie, J. Phys.: Cond. Matter **12** (2000) L735-L740.
² R. Crook, C.G. Smith, W.R. Tribe, S.J. O'Shea, M.Y. Simmons and D.A. Ritchie, Phys. Rev. B **66** (2002) 121301(R).
³ R. Crook, C.G. Smith, A.C. Graham, I. Farrer, H.E. Beere and D.A. Ritchie, Phys. Rev. Lett. **91** (2003) 246803.
⁴ A. Pioda, S. Kičín, T. Ihn, M. Sigrist, A. Fuhrer, K. Ensslin, A. Weichselbaum, S.E. Ulloa, M. Reinwald and W. Wegscheider, Phys. Rev. Lett. **93** (2004) 216801.
⁵ S. Kičín, A. Pioda, T. Ihn, M. Sigrist, A. Fuhrer, K. Ensslin, M. Reinwald and W. Wegscheider, New J. Phys. **7** (2005) 185.
⁶ A. Kumar, S. E. Laux and F. Stern, Phys. Rev. B **42** (1990) 5166.
⁷ D. Jovanovic and J.P. Leburton, Phys. Rev. B **49** (1994) 7474.
⁸ M. Stopa, Phys. Rev. B **54** (1996) 13767.

⁹ M. Governale, M. Macucci, G. Iannaccone, C. Ungarelli and J. Martorell, J. Appl. Phys. **85** (1999) 2962.
¹⁰ M. Macucci, K. Hess and G.J. Iafrate, Phys. Rev. B **48** (1993) 17354.
¹¹ M. Ferconi and G. Vignale, Phys. Rev. B **50** (1994) 14722.
¹² Y. Wang, J. Wang, H. Guo and E. Zaremba, Phys. Rev. B **52** (1995) 2738.
¹³ L. Jacak, J. Krasnyj and A. Wojs, Physica B **229** (1997) 279.
¹⁴ K. Hirose and N.S. Wingreen, Phys. Rev. B **59** (1999) 4604.
¹⁵ S.M. Reimann and M. Manninen, Rev. Mod. Phys. **74** (2002) 1283.
¹⁶ V. Shikin, T. Demel and D. Heitmann, Sov. Phys. JETP **69** (1989) 797-803.
¹⁷ V. Shikin, S. Nazin, D. Heitmann and T. Demel, Phys. Rev. B **43** (1991) 11903-7.

- ¹⁸ Z.L. Ye and E. Zaremba, Phys. Rev. B **50** (1994) 17217.
- ¹⁹ J. Martorell, Hua Wu and D.W.L. Sprung, Phys. Rev. B **50** (1994) 17298-308.
- ²⁰ S. E. Laux, J. D. Franck and F. Stern, Surf. Sci. **196** (1988) 101.
- ²¹ J. H. Davies, Semicond. Sci. Technol. **3** (1988) 995.
- ²² A.R. Long, J.H. Davies, M. Kinsler, S. Vallis and M.C. Holland, Semicond. Sci. Technol. **8** (1993) 1581.
- ²³ Hong Jiang, D. Ullmo, Weitao Yang and H.U. Baranger, Phys. Rev. B **69** (2004) 235326.
- ²⁴ I.I. Yakimenko, A.M. Bychkov and K.F. Berggren, Phys. Rev. B **63** (2001) 165309.
- ²⁵ J.H. Davies, I.A. Larkin and E.V. Sukhorukov, J. Appl. Phys. **77** (1995) 4504.
- ²⁶ O.E. Raichev and P. Debray, J. Appl. Phys. **93** (2003) 5422.
- ²⁷ M.G. Pala, G. Iannaccone, S. Kaiser, A. Schliemann, L. Worschech and A. Forchel, Nanotechnology **13** (2002) 373.
- ²⁸ G. Fiori, G. Iannaccone, M. Macucci, S. Reizenstein, S. Kaiser, M. Kesselring, L. Worschech and A. Forchel, Nanotechnology **13** (2002) 299.
- ²⁹ M. Abramowitz and I.A. Stegun, "Handbook of Mathematical Functions", Dover Publications (New York), (1965).
- ³⁰ D.W.L. Sprung and J. Martorell, Sol. State Comm. **99** (1996) 701-6.
- ³¹ E. Zaremba, Phys. Rev. B **53** (1996) R10512.
- ³² I.S. Gradshteyn and I.M. Ryzhik, "Table of Integrals, Series and Products", Academic Press 1980.

file: lepdot16.tex February 15, 2007